Numerical analysis of axially loaded circular high strength concrete-filled double steel tubular short columns

Ahmed, M., Liang, Q. Q., Patel, V. I. and Hadi, M. N. S. (2019). Numerical analysis of axially loaded circular high strength concrete-filled double steel tubular short columns. *Thin-Walled Structures*, 138: 105-116.

Numerical analysis of axially loaded circular high-strength concrete-filled double steel tubular short columns

Mizan Ahmed[a], Qing Quan Liang[a,*], Vipulkumar Ishvarbhai Patel[b], Muhammad N. S. Hadi[c]

[a] *College of Engineering and Science, Victoria University, PO Box 14428, Melbourne, VIC 8001, Australia*
[b] *School of Engineering and Mathematical Sciences, La Trobe University, Bendigo, VIC 3552, Australia*
[c] *School of Civil, Mining and Environmental Engineering, University of Wollongong, Wollongong, NSW 2522, Australia*

ABSTRACT

Circular high-strength concrete-filled double steel tubular (CFDST) columns are high performance members where the internal and external steel tubes offer significant confinement to the concrete infill. The confinement remarkably improves the concrete compressive strength and ductility. However, no fiber element models have been formulated for computing the responses of CFDST columns with circular steel tubes filled with high-strength concrete incorporating accurate confinement to the core and sandwiched concrete. In this paper, a new fiber-based numerical model is developed that computes the axial load-strain responses of circular high-strength CFDST short columns under axial loading. Based on existing experimental results, a new confining pressure model is developed for the determination of the confining pressures on the core-concrete in CFDST columns with circular sections. A new strength degradation parameter is also proposed that allows the concrete post-peak characteristics to be quantified. The fiber-based numerical model validated by experimental data is used to assess the responses of high-strength CFDST columns considering important parameters, which include the inner steel tube, external tube diameter-to-thickness ratio and

*Corresponding author. Tel.: 61 3 9919 4134.
E-mail address: Qing.Liang@vu.edu.au (Q. Q. Liang)

concrete and steel strengths. A simple expression is derived for the estimation of the axial load-carrying capacities of circular short CFDST columns and comparisons with several design codes are made. The proposed fiber-based analysis technique and design equation can accurately determine the responses of short circular high-strength CFDST columns.

Keywords: Concrete-filled double steel tubes; composite columns; high-strength concrete; numerical modeling.

1. Introduction

A circular concrete-filled double steel tubular (CFDST) column is fabricated by means of filling concrete into two concentrically-placed circular hollow steel tubes as illustrated in Fig. 1. The CFDST columns have higher ductility and strength performance than conventional circular concrete-filled steel tubular (CFST) columns because the internal steel tube offers additional confinement to the core-concrete. In addition, CFDST columns could be constructed by high-strength concrete that allows further improvement in the column ultimate strengths, but its brittleness affects the ductility of the columns. Analytical and experimental investigations on circular high-strength CFDST columns constructed by carbon steel tubes have been very limited. The confinement induced by the inner and external steel tubes to the core-concrete in CFDST columns with circular sections has not been fully understood and quantified. Furthermore, limited studies on CFDST columns have not resulted in the development of appropriate design specifications in international standards for circular CFDST columns. Therefore, it is important to propose an accurate numerical model that can accurately quantify the confinement effects in circular CFDST columns to determine the behavior of CFDST columns and propose design recommendation based on numerical solutions.

The performance of CFST columns made of circular and rectangular sections has been studied by means of conducting experiments [1-6]. Portolés et al. [3] performed testes on slender circular CFST columns exposed to eccentric loadings. It was observed from the tests that the high-strength concrete increased the strength of shorter columns under small load eccentricities. However, increasing the end eccentricity improved the column ductility. Their comparative studies showed that the strengths of eccentrically-loaded slender CFST columns calculated by the design approach given in Eurocode 4 [7] were conservative compared to test data. Similar conclusions were given by O'Shea and Bridge [4] for circular CFST short columns under combined actions. Xiong et al. [6] studied the experimental behavior of short CFST circular columns constructed by means of using ultra-high-strength concrete (UHSC). They reported that UHSC CFST short columns attained their ultimate axial strengths at small strains before the core-concrete was confined by the steel tubes. In addition, the applied loads on the UHSC CFST columns dropped sharply after the maximum load had been attained owing to the brittleness of high-strength concrete.

In comparisons with experimental studies on CFST columns, only limited experimental investigations on CFDST columns with circular sections were performed by researchers, such as Xiong et al. [6], Peng et al. [8], Liew and Xiong [9], Romero et al. [10], Wan and Zha [11], Ekmekyapar and Al-Eliwi [12]and Ibañez et al. [13]. Peng et al. [8] tested axially-loaded short CFDST circular columns to failure. The cube strengths of the filled concrete in these specimens varied from 66 MPa to 102 MPa. The diameter-to-thickness (D_o / t_o) ratios of the external tube varied from 27 to 65.4 and the internal steel tube D_i / t_i ratios ranged from 14.1 to 22.8. Experimental observations indicated that the column ultimate strengths were reduced by increasing the D_o / t_o ratios of the outer tube. Xiong et al. [6] conducted experiments on circular CFDST short columns where ultra-high-strength concrete was employed. The yield stress of

inner and outer tubes was up to 428 MPa. The compressive cylindrical strengths of the filled concrete varied from 51 to 184 MPa. It was found that CFDST short columns with circular sections had higher axial strengths than circular CFST short columns. Liew and Xiong [9] and Romero et al. [10] reported that the performance of CFDST columns was dependent on the sectional configurations of steel tubes. Filling the inner tube with ultra-high-strength concrete and the external tube with normal-strength concrete resulted in considerable improvement in the column ultimate axial strengths with superior ductility than any other combinations of concrete strength. Chang et al. [14] and Zheng et al. [15] undertook experiments on short concrete-filled stainless steel-carbon steel tubular (CFSCST) circular columns where the outer circular tube was constructed by stainless steel and the internal circular tube was made of carbon steel. Although CFSCST columns can be regarded as another form of CFDST columns, their behavior sustainably differs from that of CFDST columns.

Computational models were proposed that calculated the responses of CFST columns and double-skin CFST columns with circular sections by researchers [16-24]. Hu et al. [16], Liang and Fragomeni [18], and Lai and Varma [21] proposed confinement models for the determination of the lateral confining pressures and the post-peak strength degradation of core concrete and implemented them in the nonlinear analysis procedures for CFST columns with circular sections. Numerical studies on CFSCST columns made of circular sections were undertaken by Chang et al. [14] and Hassanein et al. [23, 24]. In these investigations, the finite element program ABAQUS was employed to create 3D models for the nonlinear analysis of CFSCST columns. The confinement models proposed for the concrete core in circular CFST columns were employed to determine the confinement induced by the internal and external tubes to the core-concrete in CFSCST columns. The stress-strain model for stainless steel obtained by the tensile coupon tests was applied to the external stainless-steel tube [25].

However, Quach et al. [26] reported that the compressive stress-strain responses of stainless steels is greatly different from the tension behavior. The adoption of the constitutive model for stainless steel based on the tensile coupon testes may lead to the underestimation of the ultimate loads of CFSCST circular columns [19].

Numerical studies on circular CFDST short column constructed by carbon steel tubes have been extremely scare [11, 27]. Wan and Zha [11] proposed a confining pressure model and a softening reduction factor as a function of confining factors for determining the post-peak responses of concrete in CFDST columns. However, it was found that the computed axial load-strain curves deviated considerably from experimental data. This highlights that further studies on the confinement mechanism are necessary and important in order to determine the actual responses of CFDST columns constructed by circular sections. Ahmed et al. [28] formulated a fiber-based mathematical model for short CFDST columns where the external tube was rectangular and the internal tube was circular. The local buckling of rectangular steel tube and concrete confinement were considered. The fiber analysis technique was demonstrated to simulate well the responses of rectangular short CFDST columns.

The above literature review shows that no fiber-based mathematical models have been proposed for the simulation of concentrically-loaded circular CFDST short columns constructed by carbon steel tubes. To accurately determine the responses of short CFDST columns made of circular sections, an accurate confinement model recognizing the effects of material properties and geometry of CFDST circular sections needs to be developed. In this paper, a fiber-based numerical method is formulated for the simulation of the axial behavior of CFDST columns with circular sections filled with high-strength concrete incorporating concrete confinement. A new formula is proposed based on experimental results for evaluating the confining pressures

on the core-concrete. An expression for the estimation of the residual concrete strength in the post-yield regime is also given. Verified by experimental results, the numerical technique is utilized to undertake a parametric study on the behavior of CFDST columns. An expression is given for calculating the column ultimate axial strengths and compared with experimental data and several design codes.

2. The fiber-based numerical model

A numerical modeling technique has been proposed based on fiber element formulations for the determination of the performance of short CFDST columns made of circular sections subjected to concentric axial loading. A column having a slenderness ratio (L/r) less than 22 is defined as a short column whose strengths are governed by its section capacities [29]. The method of fiber analysis is computationally efficient and accurate numerical technique for composite columns [28-32]. The method discretizes the cross-section of the CFDST column into many small fiber elements as illustrated in Fig. 2. Steel fibers are assigned to steel material properties while concrete fibers are assigned to concrete material properties. The assumptions of the mathematical formulation are: (a) the bond at the interface of the steel tubes and concrete is perfect; (b) the strain is lineally distributed through the cross-sectional depth; and (c) the concrete shrinkage and creep are ignored. The computational procedure starts with initializing a small strain and then calculating the fiber stresses by means of employing the uniaxial stress-strain models for concrete and steel materials. The axial force P is computed by integrating stresses over the column cross-section. The analysis is repeated by incrementally increasing the axial strain until the axial load drops to 50% of the column ultimate axial load or the specified ultimate concrete strain ε_{cu} is exceeded.

The ductility of a CFDST column in axial compression is expressed by the following indicator:

$$PI_{sd} = \frac{\varepsilon_u}{\varepsilon_y} \tag{1}$$

in which ε_u is the strain at the axial load that falls to 90% of the column ultimate strength in the post-peak range or the ultimate strain in the post-yield ascending stress-strain branch. The yield strain ε_y is calculated as $\varepsilon_{0.75} / 0.75$, where $\varepsilon_{0.75}$ represents the strain under the axial load that achieves 75% of the column ultimate axial load in the ascending branch [22, 33, 34]

3. Material model for steel tubes

The internal and external steel tubes in a CFDST column with circular section are under biaxial stresses resulting from the longitudinal compression and either hoop compression or tension which lowers the yield stress of the steel tubes. To consider this effect, the yield stress is reduced by a factor of 0.9 in the constitutive model for structural steels as shown in Fig. 3. The parabolic curve in the strain range of $0.9\varepsilon_{sy} < \varepsilon_s \le \varepsilon_{st}$ applied to cold-formed steels is defined using the expression proposed by Liang [30] as

$$\sigma_s = f_{sy}\left(\frac{\varepsilon_s - 0.9\varepsilon_{sy}}{\varepsilon_{st} - 0.9\varepsilon_{sy}}\right)^{\frac{1}{45}} \tag{2}$$

where σ_s denotes the axial steel stress; ε_s represents the axial steel strain; f_{sy} stands for the steel yield strength; ε_{sy} is the yield strain; and ε_{st} is the strain at the onset of strain-hardening

and is taken as 0.005 in the present study.

The equations given by Mander [35] are utilized to calculate the stress from the axial strain when the strain is in the range of $\varepsilon_{st} < \varepsilon_s \le \varepsilon_{su}$, written as

$$\sigma_s = f_{su} - \left(\frac{\varepsilon_{su} - \varepsilon_s}{\varepsilon_{su} - \varepsilon_{st}} \right)^n (f_{su} - f_{sy}) \tag{3}$$

$$n = E_{st} \left(\frac{\varepsilon_{su} - \varepsilon_{st}}{f_{su} - f_{sy}} \right) \tag{4}$$

in which f_{su} denotes the steel tensile strength, $\varepsilon_{su} = 0.2$ is the ultimate strain and E_{st} represents the steel modulus at the onset of strain-hardening and a value of $0.02E_s$ is used.

4. Material model for confined concrete

4.1. General stress-strain curve

The two-stage stress-strain model presented in Fig. 4 is employed to model the responses of confined concrete in CFDST columns with circular sections under axial compression. In the first stage $(0 \le \varepsilon_c \le \varepsilon_{cc}^{'})$, the following formula by Mander et al. [36] is employed to calculate the stress of the confined concrete from the axial strain:

$$\sigma_c = \frac{f_{cc}^{'}(\varepsilon_c / \varepsilon_{cc}^{'})\lambda}{(\varepsilon_c / \varepsilon_{cc}^{'})^{\lambda} + \lambda - 1} \tag{5}$$

where σ_c is the axial stress in compression and ε_c denotes the corresponding strain; $f_{cc}^{'}$ and $\varepsilon_{cc}^{'}$ represent the compressive strength and corresponding strain of the confined concrete, respectively; and λ controls the initial slope and the curvature of the ascending branch and given by

$$\lambda = \frac{\varepsilon_{cc}^{'} E_c}{\varepsilon_{cc}^{'} E_c - f_{cc}^{'}} \tag{6}$$

in which E_c represents the concrete modulus of elasticity. Lim and Ozbakkaloglu [37] derived an expression for estimating E_c by analyzing many experimental results on concrete cylinders. Their expression was modified by Ahmed et al. [28] to consider the effect of column size as follows:

$$E_c = 4400 \sqrt{\gamma_c f_c'} \text{ (MPa)} \tag{7}$$

where γ_c stands for the reduction factor applied to the concrete strength considering the influence of the column size, proposed by Liang [30] for CFST columns as

$$\gamma_c = 1.85 D_c^{-0.135} \qquad (0.85 \le \gamma_c \le 1.0) \tag{8}$$

in which D_c denotes the concrete-core diameter of circular CFST and CFDST columns, and taken as $(D_o - 2t_o)$ for sandwiched concrete and $(D_i - 2t_i)$ for core-concrete in circular CFDST columns.

In the second stage ($\varepsilon_c > \varepsilon_{cc}^{'}$), the descending stress-strain branch of confined-concrete is defined by the equation formulated by Lim and Ozbakkaloglu [37] as

$$\sigma_c = f_{cc}^{'} - \frac{f_{cc}^{'} - f_{cr}}{\left[1+\left(\frac{\varepsilon_c - \varepsilon_{cc}^{'}}{\varepsilon_{ci} - \varepsilon_{cc}^{'}}\right)^{-2}\right]} \tag{9}$$

where f_{cr} represents the concrete residual strength and ε_i denotes the concrete strain corresponding to the inflection point, which defines the shape of the stress-strain curve in the post-peak range as illustrated in Fig. 4.

Parameters studies show that the $f_{cr} / f_{cc}^{'}$ ratio is mainly influenced by the D/t ratio and $f_c^{'}$. Based on the regression analyses, an expression is proposed for $f_{cr} / f_{cc}^{'}$ as follows:

$$\frac{f_{cr}}{f_{cc}^{'}} = 1.2420 - 0.0029\left(\frac{D}{t}\right) - 0.0044\,\gamma_c f_c^{'} \qquad \left(0 \le \frac{f_{cr}}{f_{cc}^{'}} \le 1.0\right) \tag{10}$$

The accuracy of the proposed Eq. (10) for calculating the normalized residual strength of concrete ($f_{cr} / f_{cc}^{'}$) is examined in Fig. 5 against the results obtained from the parametric study on 92 test data [1, 2, 6, 8, 9, 11, 12, 38, 39].

Lim and Ozbakkaloglu [37] provided a formula for determining the strain (ε_i) at the inflection point based on extensive test results. Their formula was modified by Ahmed et al. [28] by using γ_c to incorporate the column size effect as follows:

$$\varepsilon_{ci} = 2.8\varepsilon_{cc}^{'}\left(\gamma_c f_c^{'}\right)^{-0.12}\left(\frac{f_{cr}}{f_{cc}^{'}}\right)+10\varepsilon_{cc}^{'}\left(\gamma_c f_c^{'}\right)^{-0.47}\left(1-\frac{f_{cr}}{f_{cc}^{'}}\right) \tag{11}$$

The concrete ultimate strain (ε_{cu}) as illustrated in Fig. 4 is specified and used as the stopping criterion in the numerical analysis.

4.2. Compressive strength and strain of confined concrete

As illustrated in Fig. 4, when the axial compressive concrete stress exceeds the effective strength $\gamma_c f_c^{'}$ of concrete in a CFDST column with circular section, the concrete is said to be confined by the steel tubes. This implies that the confined-concrete compressive strength increases from $\gamma_c f_c^{'}$ to the maximum value $f_{cc}^{'}$ with increasing the axial load [22]. The maximum strength ($f_{cc}^{'}$) and its corresponding strain ($\varepsilon_{cc}^{'}$) of the concrete confined are determined by the formulas provided by Mander et al. [36] incorporating the factor γ_c given by Liang and Fragomeni [18] as follows:

$$f_{cc}^{'} = \left(1+\frac{k_1 f_{rp}}{\gamma_c f_c^{'}}\right)\gamma_c f_c^{'} \tag{12}$$

$$\varepsilon_{cc}^{'} = \varepsilon_c^{'} + \frac{k_2 f_{rp}\varepsilon_c^{'}}{\gamma_c f_c^{'}} \tag{13}$$

in which f_{rp} represents the confining pressure on the concrete offered by the tubes. In the present study, $k_1 = 4.1$ and $k_2 = 20.5$ provided by Richart et al. [40] are used. The axial strain

$\varepsilon_c^{'}$ at $f_c^{'}$ depends on the effective concrete strength in compression. The following equation given by De Nicolo et al. [41] for computing the strain $\varepsilon_c^{'}$ is adopted in the present study:

$$\varepsilon_c^{'} = 0.00076 + \sqrt{(0.626\gamma_c f_c^{'} - 4.33)\times 10^{-7}} \tag{14}$$

4.3. Confining pressure model for sandwiched concrete

Experimental results showed that the outer tube of a circular CFDST column was forced to buckle locally outward and the sandwiched concrete crushed where the steel tube buckled [6, 11, 12]. The finite element analyses on circular CFST and CFDST columns conducted by Chang et al. [21] indicated that the longitudinal compressive stress in the core-concrete in the circular CFDST column was higher than that in the corresponding concrete in the CFST column. However, the longitudinal compressive stress in the sandwiched concrete in the CFDST column was similar to that in the corresponding concrete in the CFST column. This implies that in a CFDST short column under axial compression, the core-concrete is confined by both the outer and inner steel tubes but the sandwiched-concrete is confined mainly by the outer steel tube and the confinement provided by the inner steel tube on the sandwiched concrete is insignificant and can be ignored. In this study, the lateral pressure on the sandwiched concrete (f_{rpo}) in CFDST columns made of circular sections is estimated by the following expressions provided by Hu et al. [16]:

$$\frac{f_{rpo}}{f_{syo}} = \begin{cases} 0.043646 - 0.000832\left(\dfrac{D_o}{t_o}\right) & \text{for } 21.7 \le \dfrac{D_o}{t_o} \le 47 \\ 0.006241 - 0.0000357\left(\dfrac{D_o}{t_o}\right) & \text{for } 47 < \dfrac{D_o}{t_o} \le 150 \end{cases} \tag{15}$$

4.4. Proposed confining pressure model for core concrete

The confining pressure model for the core concrete was developed by means of interpreting the experimental data of 34 circular short CFDST columns given in Table 1 [6, 8-9,11-12]. The maximum axial load on the axial load-strain curve with softening was used as the ultimate axial strength of the CFDST column. For specimens without softening behavior, the axial load at the ultimate strain was assumed to reach its ultimate state. The compressive strength for the confined core-concrete was calculated by subtracting the capacities of the sandwiched concrete and internal and external steel tubes. The lateral pressure ($f_{rpi,\exp}$) on the core concrete obtained from experiments was then determined using Eq. (16). By undertaking the regression analyses on the experimental data given in Table 1, a new expression for quantifying the confining pressure exerted on the core-concrete in CFDST columns with circular sections is proposed as

$$f_{rpi} = 2.2897 + 0.0066\left(\frac{D_o}{t_o}\right) - 0.1918\left(\frac{D_i}{t_i}\right) - \left[0.0585\left(\frac{D_o}{t_o}\right) - 0.3801\left(\frac{D_i}{t_i}\right)\right]\zeta^{-1} \quad \left(f_{rpi} \geq 0\right) \tag{16}$$

in which D_i and D_o are the diameters of the internal and external steel tubes, respectively; t_i and t_0 are the thickness of the inner and outer tubes, respectively; and ζ is the confinement factor which is expressed by

$$\zeta = \frac{A_{so} f_{sy,o} + A_{si} f_{sy,i}}{A_{sc}\gamma_c f_{sc}^{'} + A_{cc}\gamma_c f_{cc}^{'}} \tag{17}$$

in which A_{so}, A_{si}, A_{sc} and A_{cc} are the cross-sectional areas of the outer tube, inner tube, sandwiched-concrete and core-concrete, respectively; $f_{cc}^{'}$ and $f_{sc}^{'}$ are the strengths of the core

concrete and sandwiched concrete in compression, respectively; f_{syi} and f_{syo} are the yield stresses of the internal and external tubes, respectively. Figure 6 shows that the lateral pressures calculated by the proposed Eq. (16) are in good correlation with test data.

5. Comparisons of computer solutions with test results

The accuracy of the fiber-based numerical model incorporating the proposed confining pressure model and material constitutive laws is established by means of comparing computations with corresponding measurements provided by Xiong et al. [6], Peng et al. [8], Liew and Xiong [9], Wan and Zha [11] and Ekmekyapar and Al-Eliwi [12]. Table 1 gives the material and geometric properties of 40 tested CFDST short columns. The unconfined concrete strengths were determined by the compression tests on concrete cubes ($f_{cu}^{'}$), concrete cylinders of 100×200 mm ($f_{c,100}^{'}$) or concrete cylinders of 150×300 mm ($f_{c}^{'}$). For consistency, the unconfined concrete strengths were converted to $f_{c}^{'}$ using the conversion of $f_{ck,100}^{'}/1.05$ and $0.85f_{cu}^{'}$, respectively.

The predicted ultimate axial loads ($P_{u,num}$) by the numerical model and the experimental values ($P_{u,\exp}$) are given in Table 2. It is observed that the fiber modeling technique accurately determines the capacities of short CFDST circular columns. The statistical study indicates that the mean $P_{u,num}/P_{u,\exp}$ ratio is calculated as 0.97 while both the coefficient of variation and standard deviation are 0.08. The simulated axial load-strain behavior of high-strength CFDST columns are provided in Fig. 7. The measured axial load-strain performance of the tested columns is determined by the mathematical model with reasonable accuracy. The experimentally measured column initial axial stiffness slightly differs from the predicted one.

The fiber-based modeling method also gives a good simulation of the post-yield responses of the CFDST columns. The discrepancy between the predictions and measurements is caused by the uncertainty of the actual concrete strength and stiffness in the tested specimens and the average concrete strength was used in the numerical analyses.

6. Parametric study

The mathematical model proposed was utilized to examine the structural behavior of short circular high-strength CFDST columns. The details on the CFDST columns under investigations are provided in Table 3. Steel tubes having the yield stresses of 250, 300, 350, 400 and 450 MPa were used in the numerical analyses and their corresponding tensile strengths were 320, 400, 420, 500 and 520 MPa, respectively. In the parametric study, the ultimate concrete strain ε_{cu} was taken as 0.04 which gives conservative results of columns with ascending stress-strain behavior in the post-yield range.

6.1. Influences of the internal steel tube

The effects of the internal tube on the strength as well as ductility of the CFDST column were examined by comparing its axial load-strain response with that of the conventional CFST column. For this purpose, analyses on Columns C1 and C2 presented in Group G1 in Table 3 were undertaken by the mathematical model. Both columns had the same outer tube diameter as well as the steel area and were made of high-strength concrete of 60 MPa. Figure 8 shows that the CFDST column has 4.85% higher strength than the CFST column due to the inclusion of the internal circular tube. The reason for the strength increase is that the inner steel tube provides additional confinement to the core-concrete, which increases the strength of the core-

concrete thereby the column ultimate strength. The CFDST column also has a better ductility than the CFST column. However, the column initial stiffness is not affected by the internal tube.

The influences of the internal tube diameter on the column behavior were evaluated by analyzing Columns C3-C6 in Group G1 in Table 3. Only the inner tube diameter (D_i) was varied in this investigation. Figure 9 presents the calculated axial loads as a function of axial strains for these CFDST columns. The ultimate axial loads of short circular CFDST columns are found to increase significantly as D_i increases. By increasing the diameter D_i from 157.5 mm to 202.5, 247.5 and 292.5 mm, the percentage increases in the column ultimate strengths are 3.4%, 7.1% and 11.4%, respectively. It would appear that increasing the diameter D_i reduces the sandwiched-concrete area but increases the core-concrete area. This implies that more concrete would be confined by the internal tube. Consequently, the strength of the CFDST column increases. Figure 9 indicates that the column initial axial stiffness is slightly affected by the inner tube diameter. The computed ductility indices of CFDST columns having different diameters are provided in Fig. 10. It would appear that circular CFDST short columns have very good ductility with a strain ductility index greater than 16.0. It is discovered that the ductility index of CFDST columns has a slight decrease as the inner steel tube diameter reduces.

Investigations were undertaken on the influences of the internal tube thickness on the behavior of CFDST columns. Columns C7-C10 in Group G1 in Table 3 with thickness ranged from 6.67 to 20 mm were analyzed. The results computed by the numerical technique are shown in Fig. 11. It appears that the ultimate axial strength of CFDST column increases considerably with increasing the thickness of the internal tube. The increase in the column ultimate strength is 14.1% when the thickness t_i is increased from 6.67 mm to 20 mm. This can be explained by the fact that increasing the inner tube thickness leads to an increase in the steel area with yield

stress of 450 MPa but the same reduction in the core-concrete area with compressive strength of 40 MPa, which results in a considerable increase in the ultimate axial strength of the column. As demonstrated in Fig. 12, reducing the thickness t_i causes a slight decrease in the ductility because of the reduction in the internal tube area. The numerical results presented in Fig. 12 indicate that when the thickness t_i is reduced from 20 mm to 15, 10 and 6.67 mm, the axial ductility index decreases from 17.40 to 17.35, 17.31 and 17.20, respectively.

It has been demonstrated that circular CFDST columns possess higher strength and ductility than circular CFST columns. High strength inner steel tubes may be used to further increase the column capacity. The use of the inner steel tube instead of reinforcing bars certainly speeds up the construction process. Moreover, the existing conventional CFST column can be strengthened by using an additional external steel tube filled with concrete and it becomes a CFDST column. However, to achieve economical and efficient designs, the cross-sections of CFDST columns must be properly designed. The proposed computational model can be used to analyze the cross-sectional capacities of CFDST columns to determine the optimal designs of CFDST columns.

6.2. Influences of D_o / t_o ratio

The behavior of CFDST columns is significantly dependent on the D_o / t_o ratios. Two scenarios were considered to examine the effects of D_o / t_o ratios. The CFDST columns with D_o / t_o ratios of 35, 40, 45 and 50 given in Group G2 in Table 3 were examined in the first scenario by changing the outer tube diameter D_o only. Figure 13 gives the computed load-strain relationships of these columns. It would appear that increasing the external steel tube diameter

D_o significantly increases the column axial strength. By increasing D_o from 280 mm to 320, 360 and 400 mm, the increases in the column axial strengths are 17.4%, 33.7% and 52.8%, respectively. This is because increasing the diameter of the outer tube increases the areas of both steel tube and concrete so that the column ultimate axial load increases. As depicted in Fig. 13, the column initial stiffness increases considerably with an increase in the D_o / t_o ratio, however, it has an insignificant impact on the post-peak responses of CFDST columns. The axial strain ductility indices are given in Fig. 14. The ductility indices are found to vary with D_o / t_o ratios. The computed axial ductility indexes are 16.3, 17.32, 18.73 and 19.63 for columns with D_o / t_o ratios of 35, 40, 45 and 50, respectively.

In the second scenario, only the external tube thickness t_o was changed to determine the D_o / t_o ratios as 35, 40, 45 and 50 as shown in Group G2 in Table 3. The axial load-strain curves predicted are given in Fig. 15. It would appear that decreasing the thickness t_o significantly decreases the column ultimate strength. The strength reductions are computed as 6.7%, 13.4% and 17.3%, respectively when the thickness t_o is reduced from 12.86 mm to 11.25, 10 and 9 mm, respectively. The reason for this is that deceasing the outer tube thickness reduces the steel tube area and the confinement on the sandwiched and core concrete so that the column axial loads decease significantly. It can be seen from Fig. 15 that the D_o / t_o ratio influences the post-yield curves. Figure 16 illustrates that increasing the D_o / t_o ratio improves the axial ductility. For CFDST short columns with D_o / t_o ratio of 35, 40, 45 and 50, the calculated strain ductility indexes are 16.05, 17.08, 18.44 and 19.06, respectively.

6.3. Influences of concrete compressive strength

In Group G3 in Table 3, the concrete of different strengths was used to construct CFDST columns. The compressive concrete strengths of 55 MPa, 75 MPa, 95 MPa and 115 MPa were considered in the fiber analysis. The predicted load-strain responses presented in Fig. 17 indicate that using higher strength concrete significantly improves the ultimate strength of CFDST columns. When $f_c^{'}$ increases from 55 MPa to 75 MPa, 95 MPa and 115 MPa, the increases in the column ultimate strengths are 13.7%, 29.2% and 44.4%, respectively. This can be explained by the fact that the ultimate axial load of short CFDST columns is governed by its section and material properties such as the concrete compressive strength. However, it is noticed that CFDST columns constructed using high-strength concrete are less ductile due to its brittle behavior.

6.4. Influences of steel yield strength

The yield stress of steel tubes has influences on the behavior of CFDST columns and its effect was studied by using the fiber-based model. The Columns in Group G4 in Table 3 were considered for this study. The calculated responses of these CFDST columns constructed by steel tubes having various yield stresses are given Fig.18. It is observed that the ultimate strength of the CFDST column significantly increases when the steel yield stress is increased. When the yield stress is increased from 250 MPa to 300 MPa, 350 MPa, 400 MPa and 450 MPa, the column ultimate strength is found to increase by 4.7%, 7.5%, 13.4% and 19.4%, respectively. The reason for the column strength increase is that the ultimate axial strength of a short CFDST column is governed by its section and material properties such as the steel yield strength. The strain ductility indices of CFDST columns are depicted in Fig. 19. It is shown that the ductility index of the column increases with an increase in its steel yield strength up to 350 MPa and after that it decreases as its steel yield strength increases.

7. Proposed design model

Currently, there are no design specifications available for the design of stub CFDST columns constructed by circular carbon steel tubes. Previously, Liang and Fragomeni [18] proposed a formula for the computation of the ultimate axial capacities of CFST columns with circular cross-sections under axial loading considering confinement effects. Liang [22] also derived design formulas for double-skin CFST short columns in axial compression. Hassanein et al. [23] recommended a formula for the design of CFSCST columns where the outer tube was made of duplex stainless steel. Based on the proposed model for lateral pressures on core-concrete and the previously cited work [18, 22], a new simple expression for the estimation of the ultimate strength of short circular CFDST columns is proposed as

$$P_{u,design} = \gamma_{so} f_{syo} A_{so} + \gamma_{si} f_{syi} A_{si} + (\gamma_{sc} f_c^{'} + 4.1 f_{rpo}) A_{sc} + (\gamma_{cc} f_c^{'} + 4.1 f_{rpi}) A_{cc} \qquad (18)$$

where γ_{so} and γ_{si} are strength factors, accounting for the influences of hoop-tension, strain hardening as well as imperfections on the outer tube and inner tube, respectively and were developed by Liang and Fragomeni [18] as

$$\gamma_{so} = 1.458\left(\frac{D_o}{t_o}\right)^{-0.1} \qquad \left(0.9 \le \gamma_{so} \le 1.1\right) \qquad (19)$$

$$\gamma_{si} = 1.458\left(\frac{D_i}{t_i}\right)^{-0.1} \qquad \left(0.9 \le \gamma_{si} \le 1.1\right) \qquad (20)$$

The proposed design equation is verified by comparing calculations with test data of 40 CFDST columns in Table 2, where $P_{u,des}$, $P_{u,\exp}$ and $P_{u,num}$ are the ultimate axial loads calculated using

Eq. (18), obtained from experiments and determined by the fiber analysis, respectively. It is observed that the mean $P_{u,des}/P_{u,\exp}$ ratio is 0.97 and the calculated coefficient of variance and standard deviation are 0.08. The strength computations of circular CFDST columns by the design model are further validated by numerical predictions in Table 3. It is shown that the strengths computed by the design model agree extremely well with corresponding numerical predictions. The proposed design formula can predict 98% of the numerical strengths with a coefficient of variance of 0.02.

8. Comparisons with design codes

The applicability of the existing design specifications for short circular CFST columns given in Eurocode 4 [7], ACI 318-11 [42] and AISC 360-16 [43] to circular CFDST columns is examined herein. Table 4 presents the specifications of the design codes to calculate the ultimate axial strengths. Eurocode 4 accounts for the influence of concrete confinement on the strength calculations of CFST circular columns whereas ACI 318-11 and AISC 360-16 neglect this effect. Table 2 summaries the comparisons between design calculations and measured results on 40 tested CFDST short columns. The calculated ultimate strengths using ACI 318-11and AISC 360-16 codes are very conservative compared to test results. Although the design method specified in Eurocode 4 yields better estimations of the load-carrying capacities of CFDST columns than ACI 318-11 and AISC 360-16, but it could not capture the actual improvement in the core concrete strength. The mean calculated-to-measured ultimate axial strengths calculated by suing Eurocode 4, ACI 318-11and AISC 360-16 are 0.89, 0.79 and 0.83, respectively. On the contrary, the proposed design model generally yields better strength predictions of short CFDST columns than design codes. The current design equation given in Eurocode 4 [7] for CFST columns is simpler than the proposed Eq. (18), but Eq. (18) yields

more accurate results than the current design provision. Further studies should focus on developing a more simple revision to the current design provision in Eurocode 4 for the design of CFDST columns.

9. Conclusions

This paper has described a fiber-based mathematical model formulated for the numerical simulations of short circular CFDST columns subjected to axial loading. A new model for computing the confining pressures on the core-concrete has been proposed based on existing test data together with a new strength-degradation parameter for quantifying the post-peak responses of confined concrete. The accuracy of the developed numerical analysis technique incorporating the new proposals of material constitutive laws has been examined by comparisons with experimental results of CFDST columns. Details parametric studies have been conducted considering various columns geometry and material properties. A new design formula has been derived and verified by test results. Furthermore, the applicability of the existing design rules recommended by Eurocode 4 [7], ACI 318-11 [42] and AISC 360-16 [43] for circular CFST columns to circular CFDST columns has been investigated.

The conclusions are given as follows:

(1) The fiber-based mathematical model developed produces predictions which are in good correlations with experimental data of circular CFDST columns under axial compression.
(2) If both circular CFDST and CFST columns have the same external tube diameter and the same steel area, the CFDST column has higher strength and ductility than the CFST column.

(3) Increasing the inner steel-tube diameter remarkably improves the ultimate strength of the CFDST column.

(4) Increasing the thickness of the inner tube considerably increases the ultimate axial loads of CFDST columns made of normal strength concrete but its effect diminishes when high-strength concrete is used.

(5) The use of higher strength steel tubes and concrete results in higher axial capacities, but it considerably affects the column axial ductility.

(6) The design rules specified in Eurocode 4 [7], ACI 318-11[42] and AISC 360-16 [43] for circular CFST columns give conservative calculations of the ultimate axial strengths of short CFDST columns made of circular steel sections.

(7) The design formula proposed yields more accurate ultimate strength predictions of CFDST columns than the design approaches provided in existing design codes.

References

[1] K. Sakino, H. Nakahara, S. Morino, I. Nishiyama, Behavior of centrally loaded concrete-filled steel-tube short columns, J. Struct. Eng. ASCE 130 (2) (2004) 180-188.

[2] G. Giakoumelis, D. Lam, Axial capacity of circular concrete-filled tube columns, J. Constr. Steel Res. 60 (7) (2004) 1049-1068.

[3] J.M. Portolés, M.L. Romero, J.L. Bonet, F.C. Filippou, Experimental study of high strength concrete-filled circular tubular columns under eccentric loading, J. Constr. Steel Res. 67 (4) (2011) 623-633.

[4] M.D. O'Shea, R.Q. Bridge, Design of circular thin-walled concrete filled steel tubes, J. Struct. Eng. ASCE 126 (11) (2000) 1295-1303.

[5] J.Y.R. Liew, M.X. Xiong, D.X. Xiong, Design of concrete filled tubular beam-columns with high strength steel and concrete, Structures 8 (2016) 213-226.

[6] M.X. Xiong, D.X. Xiong, J.Y.R. Liew, Axial performance of short concrete filled steel tubes with high-and ultra-high-strength materials, Eng .Struct. 136 (2017) 494-510.

[7] Eurocode 4, Design of Composite Steel and Concrete Structures-Part 1-1: General Rules and Rules for Buildings, European Committee for Standardization, CEN, Brussels, Belgium, 2004.

[8] Y.Y. Peng, K.F. Tan, Y. Yao, Mechanical properties of duplex steel tube high- strength concrete short columns under axial compression, J. Wuhan Uni. of Tech. 33 (2) (2011) 105-109 (In Chinese).

[9] J.Y.R. Liew, D.X. Xiong, Ultra-high strength concrete filled composite columns for multi-storey building construction, Adv. in Struct. Eng. 15 (9) (2012) 1487-1503.

[10] M.L. Romero, A. Espinós, J. Portolés, A. Hospitaler, C. Ibañez, Slender double-tube ultra-high strength concrete-filled tubular columns under ambient temperature and fire, Eng. Struct. 99 (2015) 536-545.

[11] C.Y. Wan, X.X. Zha, Nonlinear analysis and design of concrete-filled dual steel tubular columns under axial loading, Steel Comp. Struct. 20 (3) (2016) 571-597.

[12] T. Ekmekyapar, B.J. Al-Eliwi, Concrete filled double circular steel tube (CFDCST) stub columns, Eng. Struct. 135 (2017) 68-80.

[13] C. Ibañez, M.L. Romero, A. Espinos, J. Portolés, V. Albero, Ultra-high strength concrete on eccentrically loaded slender circular concrete-filled dual steel columns, Structures 12 (2017) 64-74.

[14] X. Chang, Z.L. Ru, W. Zhou, Y.B. Zhang, Study on concrete-filled stainless steel–carbon steel tubular (CFSCT) stub columns under compression, Thin-Walled Struct. 63 (2013) 125-133.

[15] Y. Zheng, C. He, L. Zheng, Experimental and numerical investigation of circular double-tube concrete-filled stainless steel tubular columns under cyclic loading, Thin-Walled Struct. 132 (2018) 151-166.

[16] H.T. Hu, C.S. Huang, M.H. Wu, Y.M. Wu, Nonlinear analysis of axially loaded concrete-filled tube columns with confinement effect, J. Struct. Eng. ASCE 129 (10) (2003) 1322-1329.

[17] E. Ellobody, B. Young, D. Lam, Behaviour of normal and high strength concrete-filled compact steel tube circular stub columns, J. Constr. Steel Res. 62 (7) (2006) 706-715.

[18] Q.Q. Liang, S. Fragomeni, Nonlinear analysis of circular concrete-filled steel tubular short columns under axial loading, J. Constr. Steel Res. 65(12) (2009) 2186-2196.

[19] V.I. Patel, Q.Q. Liang, M.N.S. Hadi, Nonlinear analysis of axially loaded circular concrete-filled stainless steel tubular short columns, J. Constr. Steel Res. 101 (2014) 9-18.

[20] F.C. Wang, L.H. Han, W. Li, Analytical behavior of CFDST stub columns with external stainless steel tubes under axial compression, Thin-Walled Struct. 127 (2018) 756-768.

[21] Z. Lai, A.H. Varma, Effective stress-strain relationships for analysis of noncompact and slender filled composite (CFT) members, Eng. Struct. 124 (2016) 457-472.

[22] Q.Q. Liang, Nonlinear analysis of circular double-skin concrete-filled steel tubular columns under axial compression, Eng. Struct. 131 (2017) 639-650.

[23] M.F. Hassanein, O.F. Kharoob, Q.Q. Liang, Behaviour of circular concrete-filled lean duplex stainless steel–carbon steel tubular short columns, Eng. Struct. 56 (2013) 83-94.

[24] M.F. Hassanein, M. Elchalakani, V.I. Patel, Overall buckling behaviour of circular concrete-filled dual steel tubular columns with stainless steel external tubes, Thin-Walled Struct. 115 (2017) 336-348.

[25] K.J. Rasmussen, Full-range stress–strain curves for stainless steel alloys, J. Constr. Steel Res. 59 (1) (2003) 47-61.

[26] W. Quach, J.G. Teng, K. Chung, Three-stage full-range stress-strain model for stainless steels, J. Struct. Eng. ASCE 134 (9) (2008) 1518-1527.

[27] D. Pons, A. Espinos, V. Albero, M.L Romero, Numerical study on axially loaded ultra-high strength concrete-filled dual steel columns, Steel and Comp. Struct. 26 (6) (2018) 705-717.

[28] M. Ahmed, Q.Q. Liang, V.I. Patel, M.N.S. Hadi, Nonlinear analysis of rectangular concrete-filled double steel tubular short columns incorporating local buckling, Eng. Struct. 175 (2018)13-26.

[29] Q.Q. Liang, Analysis and Design of Steel and Composite Structures, CRC Press, Taylor and Francis Group, Boca Raton and London, 2014.

[30] Q.Q. Liang, Performance-based analysis of concrete-filled steel tubular beam–columns, Part I: Theory and algorithms, J. Constr. Steel Res. 65 (2) (2009) 363-372.

[31] Q.Q. Liang, Performance-based analysis of concrete-filled steel tubular beam–columns, Part II: Verification and applications, J. Const. Steel Res. 65 (2) (2009) 351-362.

[32] V.I. Patel, Q.Q. Liang, M.N.S. Hadi, Concrete-filled stainless steel tubular columns, CRC Press, Taylor and Francis Group, Boca Raton and London, 2018.

[33] R. Park, Evaluation of ductility of structures and structural subassemblages from laboratory testing, Bull. New Zealand Soc. Earthq. Eng. 22(3) (1989) 155–166.

[34] Z. Tao, L.H. Han, Z.L. Zhao, Behavior of concrete-filled double skin (CHS inner and CHS outer) steel tubular stub columns and beam-columns, J. Constr. Steel Res. 60 (2004) 1129–1158.

[35] J.B. Mander, Seismic design of bridge piers, Ph.D. Thesis, Depart. of Civil Eng. Uni. of Canterbury, Christchurch, New Zealand, 1983.

[36] J.B. Mander, M.J. Priestley, R. Park, Theoretical stress-strain model for confined concrete, J. Struct. Eng. ASCE 114 (8) (1988) 1804-1826.

[37] J.C. Lim, T. Ozbakkaloglu, Stress–strain model for normal-and light-weight concretes under uniaxial and triaxial compression, Constr. Build. Mater. 2014; 71 (2014) 492-509.

[38] S.P. Schneider, Axially loaded concrete-filled steel tubes, J. Struct. Eng. 124 (10) (1998) 1125-1138.

[39] L.H. Han, G.H. Yao GH, X.L. Zhao, Tests and calculations for hollow structural steel (HSS) stub columns filled with self-consolidating concrete (SCC), J. Constr. Steel Res. 61 (9) (2005) 1241-1269.

[40] F.E. Richart, A. Brandtzaeg, R.L. Brown, A study of the failure of concrete under combined compressive stresses, Uni. of Illinois at Urbana Champaign, College of Eng. Eng. Exp. Station, 1928.

[41] B. De Nicolo, L. Pani, E. Pozzo, Strain of concrete at peak compressive stress for a wide range of compressive strengths, Mater. and Struct. 27 (4) (1994) 206-210.

[42] ACI 318-11, Building Code Requirements for Reinforced Concrete, American Concrete Intitute, Detroit (MI), 2011.

[43] AISC 360-16, Specification for Structural Steel Buildings, American Institute of Steel Construction, Chicago (IL), 2016.

Figures and tables

Table 1 Geometric and material properties of tested circular CFDST short columns.

Specimen	Outer Tube					Inner Tube					Concrete		Ref.
	$D_o \times t_o$ (mm)	$\frac{D_o}{t_o}$	$f_{sy,o}$ (MPa)	$f_{su,o}$ (MPa)	$E_{s,o}$ (GPa)	$D_i \times t_i$ (mm)	$\frac{D_i}{t_i}$	$f_{sy,i}$ (MPa)	$f_{su,i}$ (MPa)	$E_{s,i}$ (GPa)	$f'_{c,o}$ (MPa)	$f'_{c,i}$ (MPa)	
C1-1	133× 4.5	29.6	361	410	200	55.9×3.4	16.4	361	410	200	56.1	56.1	[8]
C1-2	133×4.5	29.6	361	410	200	56×3.4	16.6	361	410	200	56.1	56.1	
C2-1	132.5×3.0	44.2	361	410	200	56×3.0	18.7	361	410	200	56.1	56.1	
C2-2	132.5×3.0	44.2	361	410	200	56×3.0	18.7	361	410	200	56.1	56.1	
C2-3	132.3×3.2	41.3	361	410	200	56.1×3.2	17.5	361	410	200	79.9	79.9	
C2-4	132×3.0	44.0	361	410	200	56.1×3.2	17.5	361	410	200	79.9	79.9	
C2-5	132.1×3.1	42.6	361	410	200	56×3.4	16.5	361	410	200	86.7	86.7	
C2-6	132×3.2	41.3	361	410	200	56.1×3.0	18.7	361	410	200	86.7	86.7	
C3-1	131.8×2.1	62.8	361	410	200	54.8×2.4	22.8	361	410	200	56.1	56.1	
C3-2	130.8×2.0	65.4	361	410	200	54.2×2.6	20.8	361	410	200	56.1	56.1	
C4-1	108×4.0	27.0	361	410	200	48×3.0	16.0	361	410	200	56.1	56.1	
C4-2	106.5×2.3	46.3	361	410	200	48×3.4	14.1	361	410	200	56.1	56.1	
C5-1	107.5×3.1	34.7	361	410	200	47.6×3.0	15.9	361	410	200	56.1	56.1	
C5-2	107.6×3.1	34.7	361	410	200	47.6×3.1	15.4	361	410	200	56.1	56.1	
S3-1-1	219×5.0	43.8	377	511	205	114×3.6	31.7	406	505	213	51	51	[9]
S3-1-2	219×5.0	43.8	377	511	205	114×3.6	31.7	406	505	213	167	167	
S3-1-3	219×5.0	43.8	377	511	205	114×3.6	31.7	406	505	213	51	167	
S3-1-4	219×5.0	43.8	377	511	205	114×3.6	31.7	406	505	213	51	184	
S3-2-1	219×10	21.9	381	509	212	114×6.3	18.1	428	521	209	51	51	
S3-2-2	219×10	21.9	381	509	212	114×6.3	18.1	428	521	209	167	167	
S3-2-3	219×10	21.9	381	509	212	114×6.3	18.1	428	521	209	51	167	
S3-2-4	219×10	21.9	381	509	212	114×6.3	18.1	428	521	209	51	184	
A1-1	426×7.73	55.1	298	408	206	133×6.6	20.2	331.4	478	200	25.9	25.9	[11]
A2-1	426×7.52	56.6	302	407	206	133×6.6	20.2	460	683	200	25.9	25.9	
A1-2	426×7.52	56.6	302	407	206	219×6.7	32.7	316.8	460	200	25.9	25.9	
A2-2	426×7.52	56.6	302	407	206	219×6.7	32.7	478	660	200	25.9	25.9	
A1-3	426×7.52	56.6	302	407	206	273×6.5	42.0	322	415	200	25.9	25.9	
A2-3	426×7.52	56.6	302	407	206	273×6.5	42.0	447	626	200	25.9	25.9	
CC1-SC1-OT1	139.7×3.3	42.3	290	350	200	88.9×4.25	20.9	375	450	200	29.1	29.1	[12]
CC1-SC1-OT2	139.7×5.9	23.7	355	410	200	88.9×4.25	20.9	375	450	200	29.1	29.1	
CC1-SC2-OT1	139.7×3.3	42.3	290	350	200	88.9×4.25	20.9	375	450	200	64.9	29.1	
CC1-SC2-OT2	139.7×5.9	23.7	355	410	200	88.9×4.25	20.9	375	450	200	64.9	29.1	
CC2-SC1-OT1	139.7×3.3	42.3	290	350	200	88.9×4.25	20.9	375	450	200	29.1	64.9	
CC2-SC1-OT2	139.7×5.9	23.7	355	410	200	88.9×4.25	20.9	375	450	200	29.1	64.9	
CC2-SC2-OT1	139.7×3.3	42.3	290	350	200	88.9×4.25	20.9	375	450	200	64.9	64.9	
CC2-SC2-OT2	139.7×5.9	23.7	355	410	200	88.9×4.25	20.9	375	450	200	64.9	64.9	
DC-09	219.1×6.3	34.8	300	467	202	114×6.3	18.1	428	519	209	155	155	[6]
DC-10	219.1×6.3	34.8	300	467	202	114×6.3	18.1	428	519	209	167	167	
DC-11	219.1×6.3	34.8	300	467	202	114×6.3	18.1	428	519	209	142	142	
DC-12	219.1×6.3	34.8	300	467	202	114×6.3	18.1	428	519	209	166	166	

Table 2 Ultimate axial strengths of circular CFDST short columns.

Specimen	$P_{u,\exp}$ (kN)	$P_{u,num}$ (kN)	$P_{u,EC4}$ (kN)	$P_{u,ACI}$ (kN)	$P_{u,AISC}$ (kN)	$P_{u,des}$ (kN)	$\frac{P_{u,num}}{P_{u,\exp}}$	$\frac{P_{u,EC4}}{P_{u,\exp}}$	$\frac{P_{u,ACI}}{P_{u,\exp}}$	$\frac{P_{u,AISC}}{P_{u,\exp}}$	$\frac{P_{u,des}}{P_{u,\exp}}$
C1-1	1942	1818	1847	1407	1455	1823	0.94	0.95	0.72	0.75	0.94
C1-2	1911	1818	1846	1407	1455	1823	0.95	0.97	0.74	0.76	0.95
C2-1	1683	1409	1546	1196	1249	1425	0.84	0.92	0.71	0.74	0.85
C2-2	1592	1409	1546	1196	1249	1425	0.89	0.97	0.75	0.78	0.90
C2-3	1831	1730	1852	1470	1544	1781	0.94	1.01	0.80	0.84	0.97
C2-4	1875	1694	1811	1442	1516	1718	0.90	0.97	0.77	0.81	0.92
C2-5	1870	1813	1916	1532	1612	1837	0.97	1.02	0.82	0.86	0.98
C2-6	1925	1831	1908	1524	1605	1853	0.95	0.99	0.79	0.83	0.96
C3-1	1434	1214	1327	1042	1097	1231	0.85	0.93	0.73	0.77	0.86
C3-2	1425	1190	1303	1026	1080	1204	0.84	0.91	0.72	0.76	0.84
C4-1	1432	1276	1042	979	1009	1281	0.89	0.73	0.68	0.70	0.89
C4-2	1106	931	875	810	842	948	0.84	0.79	0.73	0.76	0.86
C5-1	1256	1110	947	883	915	1121	0.88	0.75	0.70	0.73	0.89
C5-2	1182	1110	953	888	920	1126	0.94	0.81	0.75	0.78	0.95
S3-1-1	3626	4051	3460	3207	3351	3790	1.12	0.95	0.88	0.92	1.05
S3-1-2	8529	7834	7295	6467	6938	8022	0.92	0.86	0.76	0.81	0.94
S3-1-3	4968	4950	4499	4091	4323	5014	1.00	0.91	0.82	0.87	1.01
S3-1-4	5239	5175	4652	4220	4465	5193	0.99	0.89	0.81	0.85	0.99
S3-2-1	6300	6558	4891	4670	4783	5918	1.04	0.78	0.74	0.76	0.94
S3-2-2	9817	8943	8252	7526	7930	9211	0.91	0.84	0.77	0.81	0.94
S3-2-3	7022	6798	5828	5466	5660	6897	0.97	0.83	0.78	0.81	0.98
S3-2-4	7160	6794	5966	5583	5788	7041	0.95	0.83	0.78	0.81	0.98
A1-1	8142	8804	7260	6756	7043	7410	1.08	0.89	0.83	0.87	0.91
A2-1	9830	9079	7563	7057	7341	7720	0.91	0.76	0.71	0.74	0.78
A1-2	9830	9383	7725	7227	7506	7956	0.95	0.79	0.74	0.76	0.81
A2-2	10025	10189	8446	7947	8216	8586	1.02	0.84	0.79	0.82	0.86
A1-3	9740	9767	8037	7542	7818	8275	1.00	0.83	0.77	0.80	0.85
A2-3	10739	10801	8717	8222	8488	8755	1.01	0.81	0.77	0.79	0.82
CC1-SC1-OT1	1435.05	1460	1306	1247	1282	1429	1.02	0.91	0.87	0.89	1.00
CC1-SC1-OT2	1977.94	2090	1658	1605	1635	1972	1.06	0.84	0.81	0.83	1.00
CC1-SC2-OT1	1606.89	1673	1514	1412	1475	1661	1.04	0.94	0.88	0.92	1.03
CC1-SC2-OT2	2044.44	2278	1908	1817	1871	2237	1.11	0.93	0.89	0.92	1.09
CC2-SC1-OT1	1570.15	1627	1415	1328	1381	1563	1.04	0.90	0.85	0.88	1.00
CC2-SC1-OT2	2153.11	2255	1849	1767	1815	2182	1.05	0.86	0.82	0.84	1.01
CC2-SC2-OT1	1784.39	1839	1704	1574	1655	1877	1.03	0.96	0.88	0.93	1.05
CC2-SC2-OT2	2274.77	2374	2099	1979	2051	2448	1.04	0.92	0.87	0.90	1.08
DC-09	7640	7346	7038	6309	6727	7504	0.96	0.92	0.83	0.88	0.98
DC-10	7209	7699	7414	6629	7078	7878	1.07	1.03	0.92	0.98	1.09
DC-11	6882	6961	6631	5963	6346	7100	1.01	0.96	0.87	0.92	1.03
DC-12	8375	7699	7383	6602	7049	7847	0.92	0.88	0.79	0.84	0.94
Mean							0.97	0.89	0.79	0.83	0.95
Standard Deviation (SD)							0.08	0.08	0.06	0.07	0.08
Coefficients of Variance (COV)							0.08	0.09	0.08	0.08	0.08

Table 3 Geometric and material properties of circular CFDST short columns utilised in the parametric study.

Group	Column	Outer tube				Inner tube				Concrete	Ultimate strength		
		D_o (mm)	t_o (mm)	$\frac{D_o}{t_o}$	f_{syo} (MPa)	D_i (mm)	t_i (mm)	$\frac{D_i}{t_i}$	f_{syi} (MPa)	f_c' (MPa)	$P_{u,num}$ (kN)	$P_{u,des}$ (kN)	$\frac{P_{u,des}}{P_{u,num}}$
G1	C1	500	12.88	38.8	350	-	-	-	-	60	18973	18387	0.97
	C2	500	10	50	350	280	5	56	350	60	19751	19849	1.00
	C3	450	10	45	350	157.5	8	19.68	350	60	14831	14696	0.99
	C4	450	10	45	350	202.5	8	25.31	350	60	15330	15249	0.99
	C5	450	10	45	350	247.5	8	30.93	350	60	15889	15868	1.00
	C6	450	10	45	350	292.5	8	36.56	350	60	16520	16534	1.00
	C7	600	10	60	450	200	6.67	30	450	40	21648	20403	0.94
	C8	600	10	60	450	200	10	20	450	40	22343	21168	0.95
	C9	600	10	60	450	200	15	13.33	450	40	23520	22396	0.95
	C10	600	10	60	450	200	20	10	450	40	24694	23559	0.95
G2	C11	280	8	35	350	140	5	28	350	60	7180	7127	0.99
	C12	320	8	40	350	140	5	28	350	60	8428	8417	1.00
	C13	360	8	45	350	140	5	28	350	60	9601	9607	1.00
	C14	400	8	50	350	140	5	28	350	60	10968	11000	1.00
	C15	450	9	50	350	200	8	25	350	70	15806	15844	1.00
	C16	450	10	45	350	200	8	25	350	70	16568	16523	1.00
	C17	450	11.25	40	350	200	8	25	350	70	17840	17683	0.99
	C18	450	12.86	35	350	200	8	25	350	70	19123	18966	0.99
G3	C19	480	12	40	350	200	8	25	350	55	18311	17655	0.96
	C20	480	12	40	350	200	8	25	350	75	20817	20537	0.99
	C21	480	12	40	350	200	8	25	350	95	23653	23420	0.99
	C22	480	12	40	350	200	8	25	350	115	26449	26302	0.99
G4	C23	720	12	60	250	280	8	35	250	60	31692	30722	0.97
	C24	720	12	60	300	280	8	35	300	60	33175	31866	0.96
	C25	720	12	60	350	280	8	35	350	60	34072	33229	0.98
	C26	720	12	60	400	280	8	35	400	60	35949	34729	0.97
	C27	720	12	60	450	280	8	35	450	60	37836	36319	0.96
Mean													0.98
Standard Deviation (SD)													0.02
Coefficients of Variance (COV)													0.02

Table 4 Design formulas for circular CFDST short columns given in design codes.

Design codes	Design equations
Eurocode 4 [7]	Circular CFST columns: $P_{u,outer} = \eta_a A_{so} f_{syo} + A_{sc} f_{sc}(1+\eta_c \frac{t_o}{D_o} \frac{f_{syo}}{f_{sc}})$ $P_{u,inner} = \eta_a A_{si} f_{syi} + A_{cc} f_{cc}(1+\eta_c \frac{t_i}{D_i} \frac{f_{syi}}{f_{cc}})$ $P_{EC4} = P_{u,outer} + P_{u,inner}$ $\eta_a = 0.25(3+2\bar{\lambda}) \quad (\eta_a \le 1.0)$ $\eta_c = 4.9 - 18.5\bar{\lambda} + 17\bar{\lambda}^2 \quad (\eta_c > 0)$ where the relative slenderness ratio is $\bar{\lambda} = \sqrt{\frac{N_{pl,Rk}}{N_{cr}}}$
ACI 318-11 [42]	$P_{u,ACI} = A_{so} f_{syo} + 0.85 A_{sc} f_{sc} + A_{si} f_{syi} + 0.85 A_{cc} f_{cc}$
AISC 360-16 [43]	$P_{u,AISC} = \begin{cases} P_o\left[0.658^{(P_o/P_e)}\right] & \text{for } P_e \ge 0.44P_o \\ 0.877P_e & \text{for } P_e < 0.44P_o \end{cases}$ $P_o = A_{so} f_{syo} + C_2 A_{sc} f_{sc} + A_{si} f_{syi} + C_2 A_{cc} f_{cc}$ $P_e = \frac{\pi^2}{(KL)^2}(EI)_{eff}$ $(EI)_{eff} = E_{so} I_{so} + E_{si} I_{si} + C_4 E_{sc} I_{sc} + C_4 E_{cc} I_{cc}$ $C_4 = 0.6 + 2\left(\frac{A_s}{A_s + A_c}\right) \le 0.9$ C_2=0.95 for circular section

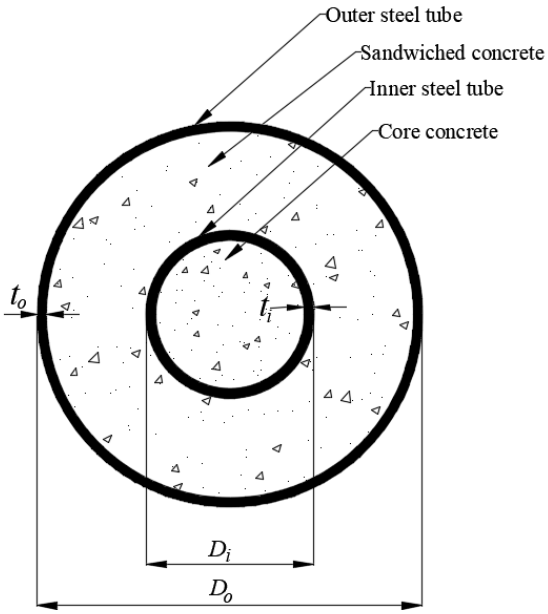

Fig. 1. Cross-section of circular CFDST column.

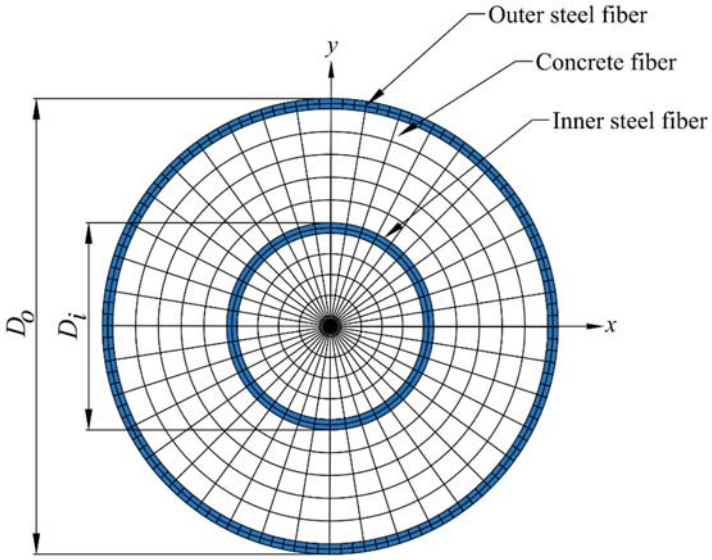

Fig. 2. Typical discretization of circular CFDST column section in the fiber element analysis.

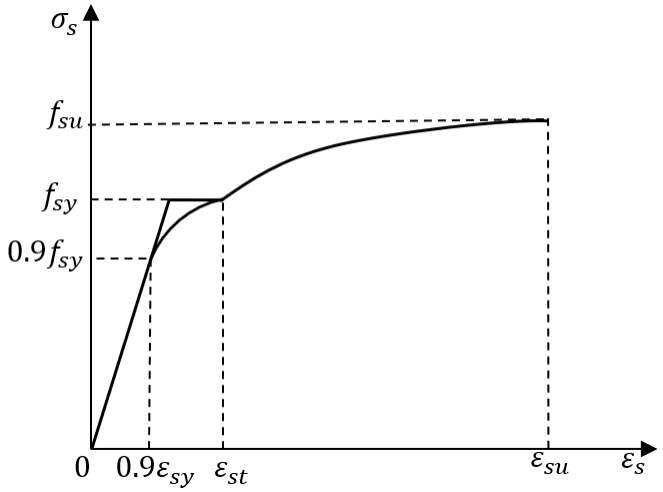

Fig. 3. General material stress-strain curve for structural steels.

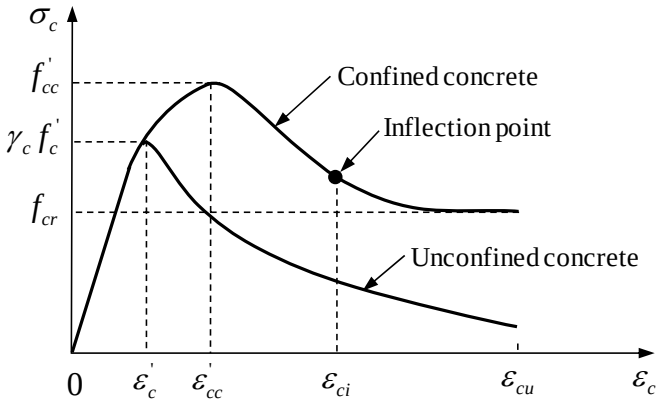

Fig. 4. Stress-strain curves for confined concrete in circular CFDST columns.

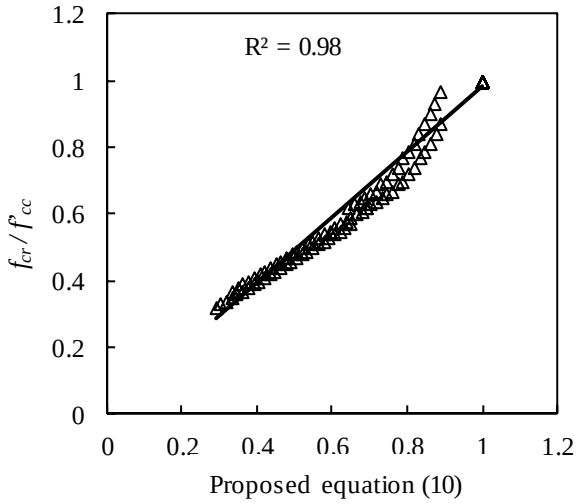

Fig. 5. Verification of the proposed expression for determining the residual concrete strength.

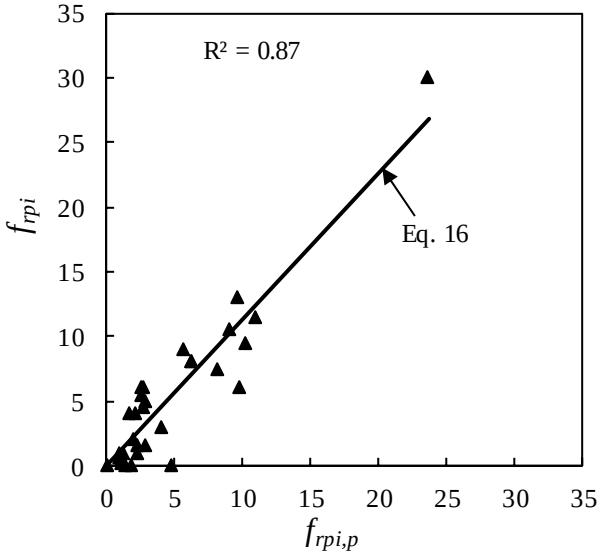

Fig. 6. Verification of the proposed expression for determining the lateral pressure on core concrete with the test results.

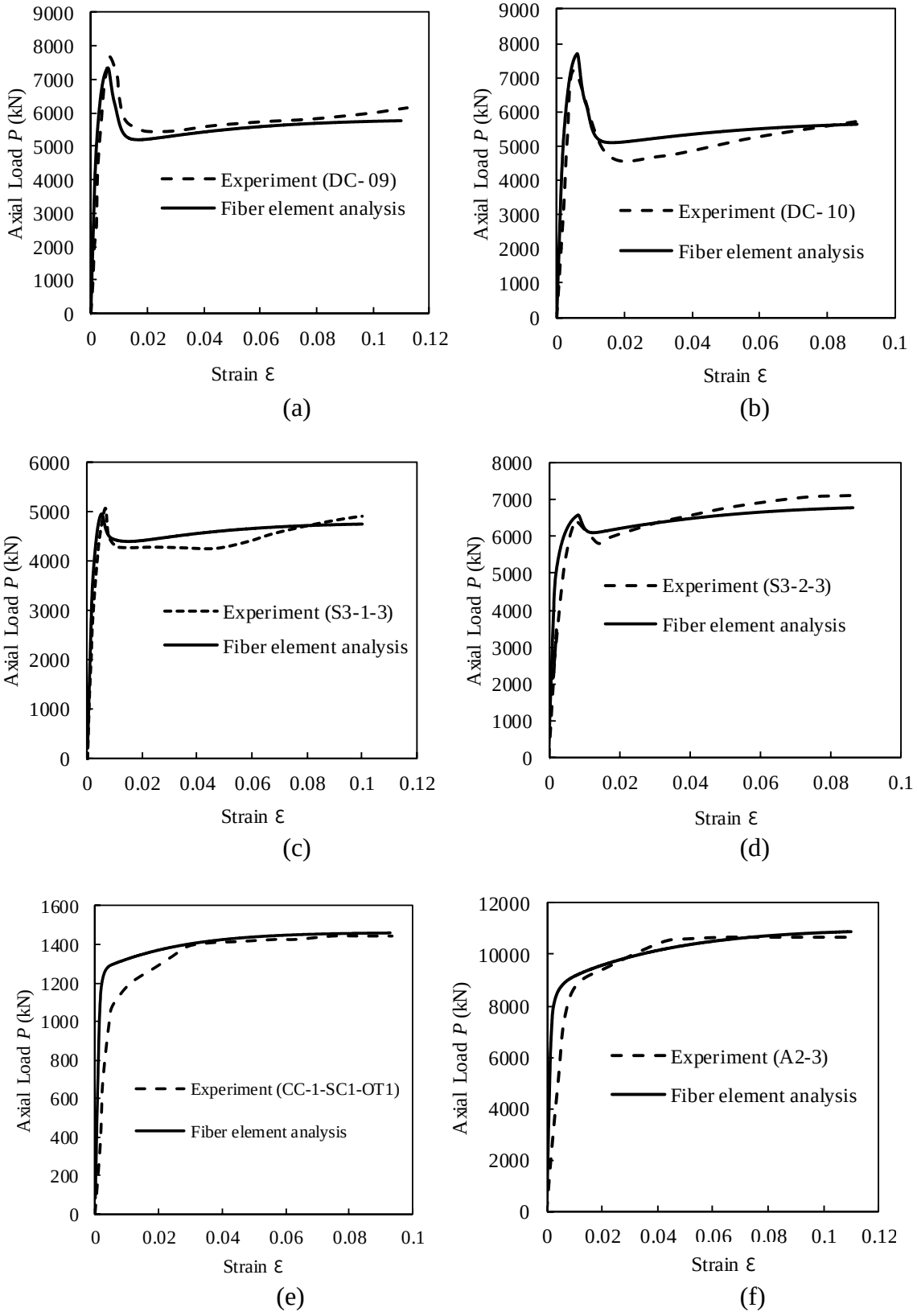

Fig. 7. Comparison of computational and experimental axial load-strain curves for circular CFDST short columns.

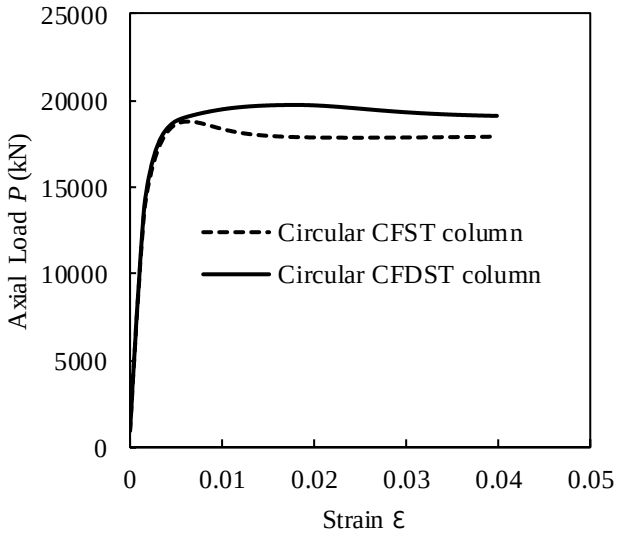

Fig. 8. Effects of the inner steel tube on the axial load-strain curves.

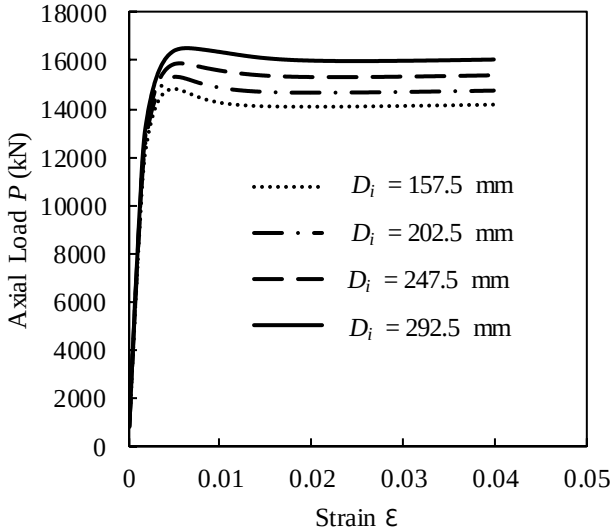

Fig. 9. Effects of the diameter of the inner steel tube on the axial load-strain curves of circular CFDST short columns.

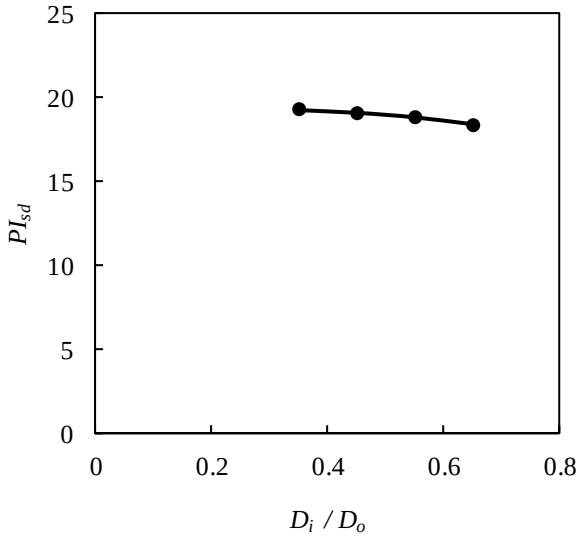

Fig. 10. Effects of D_i/D_o ratio on the strain ductility index of circular CFDST short columns.

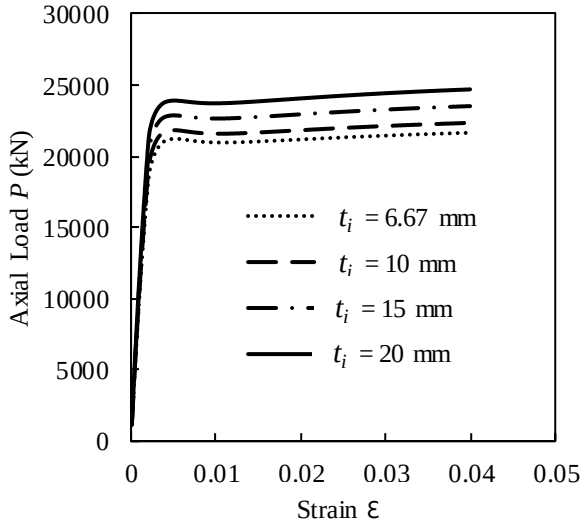

Fig. 11. Effects of the thickness of the inner steel tube on the axial load-strain curves of circular CFDST short columns.

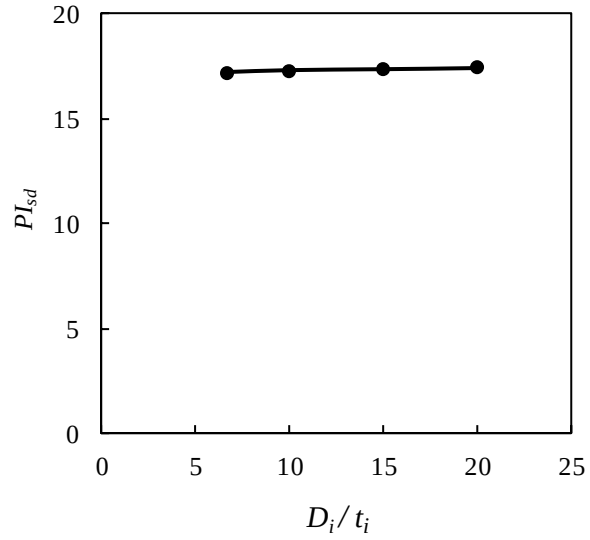

Fig. 12. Effects of D_i / t_i ratio on the strain ductility index of circular CFDST short columns.

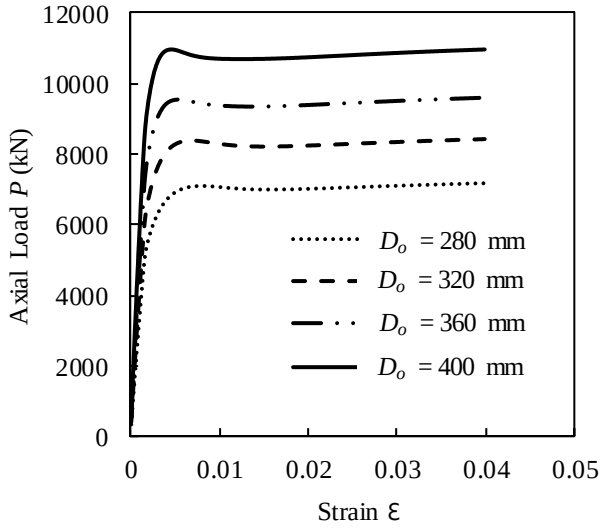

Fig. 13. Effects of the diameter of the outer steel tube on the axial load-strain curves of circular CFDST short columns.

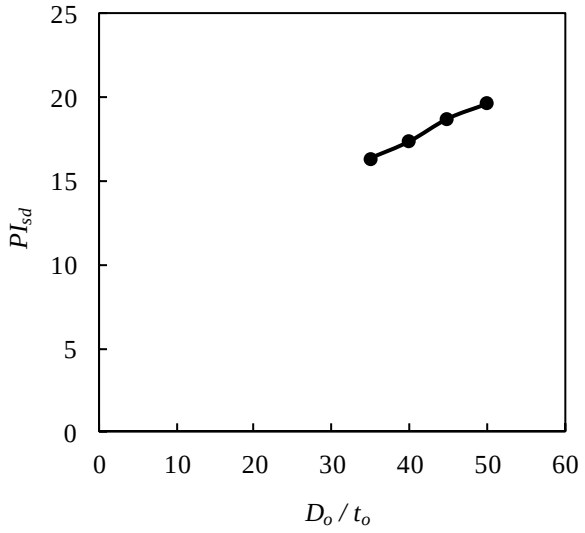

Fig. 14. Effects of D_o/t_o ratio by varying diameter of the outer steel tube on the strain ductility index of circular CFDST short columns.

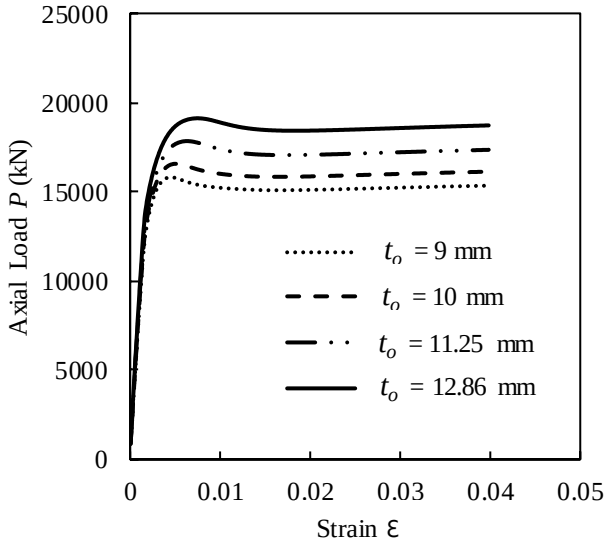

Fig. 15. Effects of the thickness of the outer steel tube on the axial load-strain curves of circular CFDST short columns.

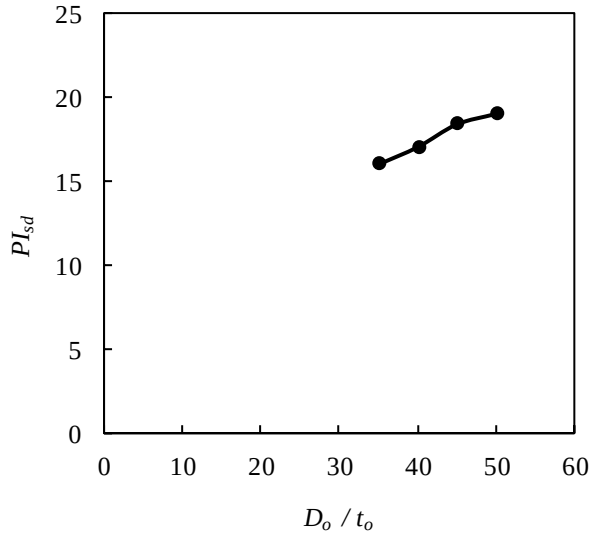

Fig. 16. Effects of D_o/t_o ratio by varying thickness of the outer steel tube on the strain ductility index of circular CFDST short columns.

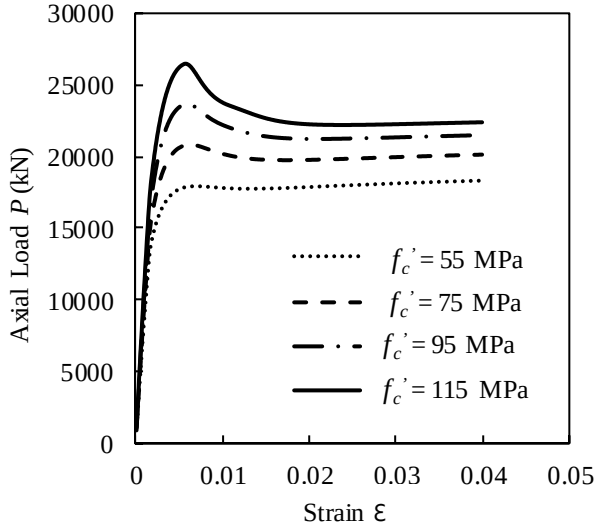

Fig. 17. Effects of concrete compressive strength on the axial load-strain curves of circular CFDST short columns.

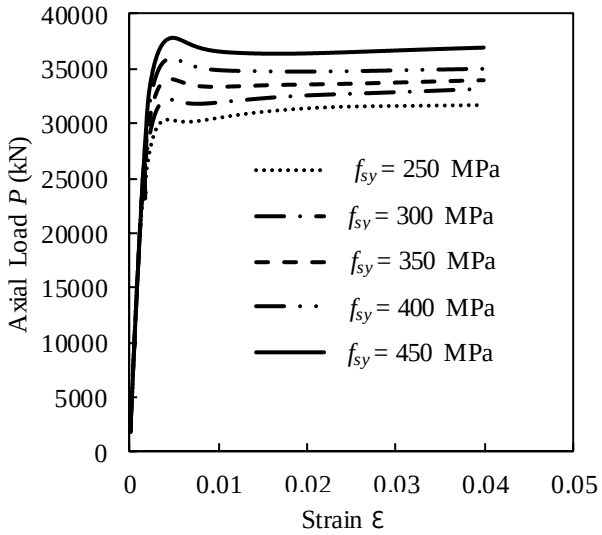

Fig. 18. Effects of steel yield strength on the axial load-strain curves of circular CFDST short columns.

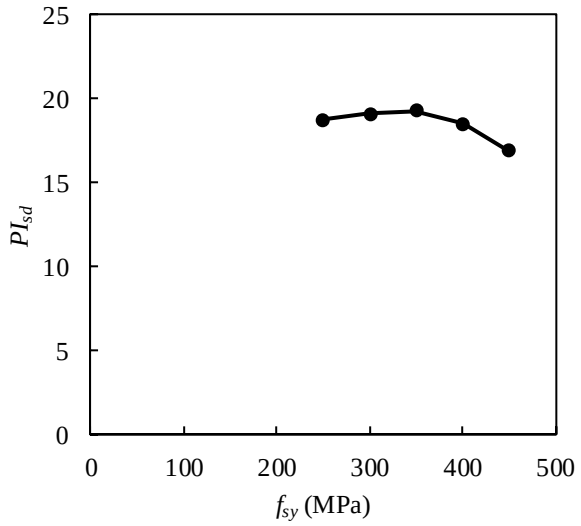

Fig. 19. Effects of steel yield strength on the strain ductility index of circular CFDST short columns.